Direct laser interference ablating nanostructures on organic crystals

Hong-Hua Fang,[1] Ran Ding,[1] Shi-Yang Lu,[1] Lei Wang,[1] Jing Feng,[1,3] Qi-Dai Chen,[2] and Hong-Bo Sun[2,4]

[1]*State Key Laboratory on Integrated Optoelectronics, College of Electronic Science and Engineering, Jilin University, 2699 Qianjin Street, Changchun 130012, China*

[2]*College of Physics, Jilin University, Changchun 130012, China*

[3]*e-mail: jingfeng@jlu.edu.cn*

[4]*e-mail: hbsun@jlu.edu.cn*

Received September 6, 2011; revised November 23, 2011; accepted December 23, 2011; posted December 23, 2011 (Doc. ID 153655); published February 14, 2012

Two-beam interference ablation of 1,4-Bis(4-methylstyryl)benzene organic crystal by short laser pulses (10 ns, 355 nm) is presented. The influence of laser fluence, interference period, and pulse number on the morphology have been studied. The morphology is closely associated with the molecular interactions in the crystals, and it could be well controlled by adjusting the laser fluence and pulses number. Through interference ablating the crystals with high fluence pulses, and then treated with low fluence laser pulses, grating structures with smooth surface could be fabricated without any additional process.

OCIS codes: 160.4890, 140.3390.

Organic crystals have attracted attention in the field of organic electronics and photonics applications because of their high stimulated cross-sections [1], large and ultrafast nonlinear responses [2,3], and carrier mobility [4]. The superiorities of organic crystals, such as high thermal stability, highly ordered structure, and high carrier mobility, make them attractive candidates for optoelectronic devices such as optically pumped lasers [5], field-effect transistors [6], and photovoltaic cells [7]. However, because of their sensitivity to the organic solvent and their fragility, most organic crystals are difficult to handle; thus, their applications are limited to simple devices. Laser ablation, as a dry technique, has been demonstrated as a powerful tool for structuring metals [8–9], insulating polymers [10,11] and inorganic semiconductors [12], and gallium arsenide [13]. However, the ablations of organic crystals are seldom reported [14]. In contrast to the inorganic counterparts, organic crystals are held together by van der Waals forces, which are much weaker than that of covalent bonds binding the atoms of inorganic semiconductors. This fundamental difference in the strength of the binding force can be expected to entail large differences in the mechanical properties and the ablation morphology.

In this work, nanosecond laser interference ablation (LIA) of 1,4-Bis(4-methylstyryl)benzene (BSB-Me) crystals was investigated. The ablated morphology shows great difference with polymer and inorganic semiconductors. The specific topography of BSB-Me crystals associated with the molecule interactions in the crystals was studied. It was demonstrated that by optimization of the laser fluence and the number of applied pulses, gratings with a smooth surface could be produced within a large area without any additional process.

The organic crystals used in this work are BSB-Me, a typical optoelectronic functional material [15]. High-quality organic crystals were grown according to a method described in a previous study [16]. Figure 1a shows the molecular structure and a photograph of a typical BSB-Me crystal under day light. The size was about 1×1 cm. The symmetry of crystal is orthorhombic with unit cell parameters $a = 7.36$ Å, $b = 5.88$ Å, $c = 38.95$ Å; $\alpha = 90°$, $\beta = 90°$, $\gamma = 90°$. For ablation, the free-standing crystal film was transferred and adhered onto the substrate. Figure 1(c) shows the ablation experiment's setup. Third harmonic generation (355 nm) of a commercial Nd:YAG nanosecond-pulsed laser (Quanta-Ray Lab, Spectra Physics) with repetition rates 10 Hz, pulse duration 10 ns, and energies in excess of 200 mJ/pulse was used. The interference of the beams results in a periodic intensity distribution, and the interference period (P) is determined by the equation $P = \lambda/(2 \sin \theta)$, where θ is the half angle of two incident beams that intersect, and λ is the laser wavelength. The constructive and destructive interference of the two beams defined a pattern of dark and

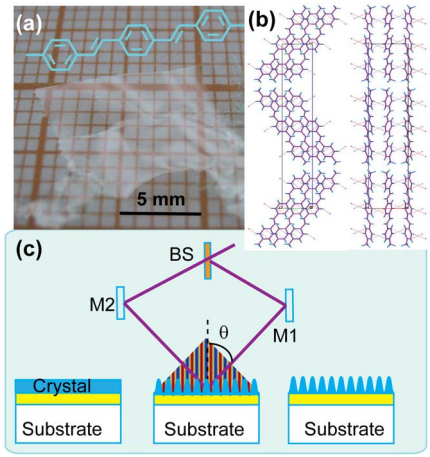

Fig. 1. (Color online) (a) Molecular structure and photograph of a typical BSB-Me crystal grown in our laboratory. (b) Crystal packing image of BSB-Me crystal. (c) The optical layout of the experimental setup for the interference ablation.

bright lines. The crystal located at the bright fringes of the interference pattern is "burned" and removed, while the materials at the dark fringes remain unremoved, forming the gratings on the crystal surface.

Presented in Fig. 2 are the SEM images of BSB-Me crystals ablated with different laser power levels and for different periods. Figure 2(a) shows the results after LIA with 100 pulses ($N = 100$) and for 400 nm grating period ($P = 400$ nm) at near-damage-threshold fluence of $F = 0.1$ J/cm^2, where the characteristic features are random nanoparticles with sizes down to about hundreds of nanometers. When the laser fluence was increased to 0.13 J/cm^2, line arrays formed and could be clearly observed, while the lines consisted of nanoparticles with sizes of 100–200 nm [Fig. 2(b)]. As the laser power was further increased, the crystals began to crack [Fig. 2(c)]. The surface topography also showed great differences when the laser interference period (P) was adjusted. Figure 2(d)–(f) shows the images at $F = 0.14$, 0.2, 0.25 J/cm^2, respectively, for $P = 2000$ nm. Large nanoribbons could be found on the surface when $F = 0.14$ J/cm^2. As the laser power was increased to 0.2 J/cm^2, some of the grating ridges were fractured and peeled off, although the grooves were ablated deeper [Fig. 2(e)]. When the laser power was further increased, most of the grating ridges were peeled off directly [Fig. 2(f)]. These suggest that increasing the laser power is not an option because of the fragility of the crystal. It is essential to fabricate the crystal devices using low laser power to avoid harmful cracks.

Laser-induced surface topography depends not only on the laser fluence but also on the number of applied pulses. Figure 3(a)–(c) shows the results produced following treatment at $F = 0.14$ J/cm^2 for various N, where the period is 2000 nm. Figure 3(d)–(f) shows the corresponding magnified image. At this middle-level laser fluence, large nanoribbons similar to those in Fig. 2(d) could be found on the surface after 50-shot treatment, as shown in Fig. 3(d). The size of these pieces is in the range 100–1000 nm according to the SEM measurements, which cover the surface of the grating structures. With further increases in the number of laser shots, it was noted that the density of the fragments were reduced greatly, and the grating structure continued to develop with deepening of the grooves [Fig. 3(b) and 3(e)]. Figure 3(c) and 3(f) show the morphology after treatment with $N = 150$ applied pulses; the fragments were almost cleaned out and the grating grooves had rapidly become broader and deeper. Upon careful observation of the grating ridge, one might find that it is composed of layer structures.

The results were further investigated by changing the ablation period from 2000 nm to 500 nm. As in the Fig. 3(g)–3(l), fragments of the crystals could also be found on the grating surface, and the density of the crystal fragments was reduced as the number of applied pulses N increased. The morphology of the fragments is very different from that in Fig. 3(a). The size of the fragments is much smaller than that in Fig. 3(a). It was noted that irregular fragments (nanoflakes) formed when the number of applied pulses increased, as seen in Fig. 3(h) and 3(k).

The fragments (nanoribbons, nanoparticles, and nanoflakes) and the grating ridge show special features, which are different from those of inorganic materials and polymers. These differences may arise from the different molecular interactions in the crystal [17]. Figure 1(b) shows the crystal packing image viewed along the a-axis and b-axis. The analysis of the crystal structures demonstrates that the molecules are arranged layer by layer in the well-known herringbone structure, laterally spreading along the ab-plane, and the long c-axis is parallel to the crystal z-axis. Three types of aromatic CH/π hydrogen bonds are formed between two molecules. Each BSB-Me molecule connects with four adjacent molecules through these three aromatic CH/π hydrogen bonds. The strong supramolecular interactions not only make the molecules

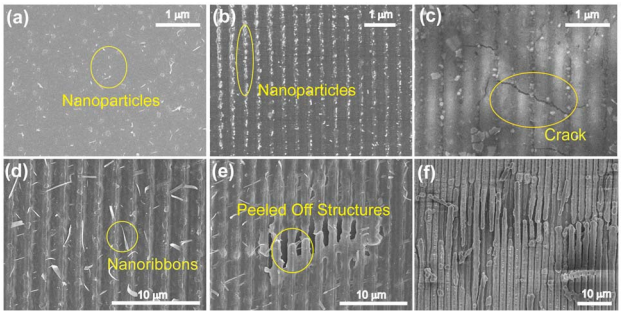

Fig. 2. (Color online) SEM pictures of BSB-Me following UV nanosecond laser interference ablation treatment at (a) $F = 0.10$ J/cm^2, period ~400 nm; (b) 0.14 J/cm^2; (c) 0.2 J/cm^2; (d) 0.14 J/cm^2, period ~2000 nm; and (e) 0.2 J/cm^2; (f) 0.25 J/cm^2.

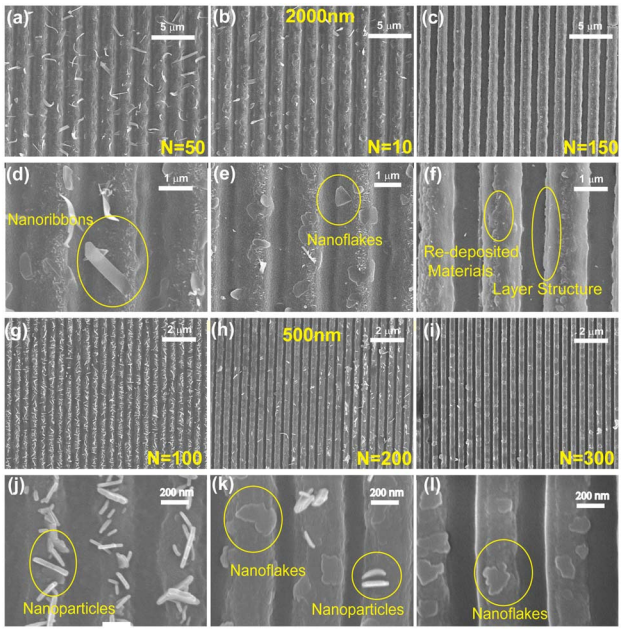

Fig. 3. (Color online) (a)–(f) SEM images of BSB-Me following UV nanosecond laser interference ablation treatment at $F = 0.14$ J/cm^2, period ~2000 nm, with various numbers of applied pulses N. (a) $N = 50$; (b) $N = 100$; (c) $N = 150$. (d), (e), and (f) are magnified views of a section in (a), (b), and (c), respectively. (g)–(l) SEM images after ablation treatment at $F = 0.14$ J/cm^2, period ~500 nm, (g) $N = 100$; (h) $N = 200$; (i) $N = 300$. (j), (k), and (l) are magnified views of a section in (g), (h), and (i), respectively.

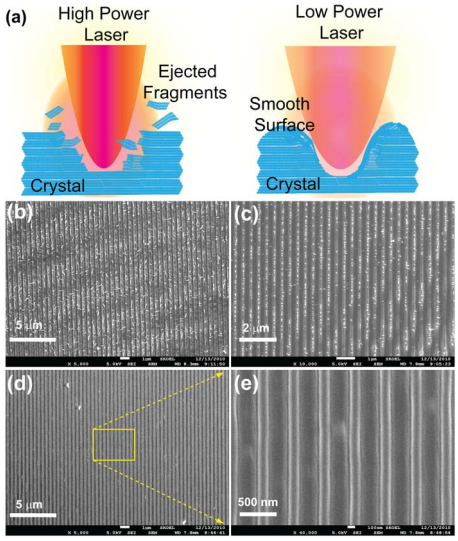

Fig. 4. (Color online) (a) Schematic picture of laser ablation process. (b) SEM picture of BSB-Me with laser interference ablation treatment at $F = 0.14$ J/cm^2, period ~400 nm, $N = 50$. Smoothed surface treated with low-power laser $F = 0.11$ J/cm^2, (c) $N = 200$,(d) $N = 500$. (e) Magnified view of a section in (d).

more rigid and stable in the crystal lattice but also induce tight intermolecular packing; as a result, the molecules assemble themselves into rigid three-dimensional supramolecular interaction networks. In this network, the interactions within each layer are strong, while the interactions between layers are weak. Thus, it could be deduced that the materials most likely break at these positions during the transient interaction between the intensive UV laser pulse and the crystals. Large amounts of fragments were produced from the crystals layer by layer, rapidly ejected, and, accompanied with thermal melting, evaporated. The size of the fragments is closely associated with the interference period, which defined the distance between the fringes of the laser interference pattern. At the bright fringes of the pattern, the laser power is strongest and the crystals undergo extreme stress. Large fragments (such as nanoribbon-like fragments) were peeled off when the period was long enough. Small fragments were produced as the period was reduced.

It was noted that in BSB-Me crystal ablation, a high laser power usually produced a large number of fragments and deep grooves, while a low laser power induced less fragments and shallow grooves. The organic crystal materials could be melted under irradiation by a low-power laser. The irregular nanoflakes may show evidence of the thermal effect. These are possibly converted from the original fragments of the crystals. In order to improve the morphology of the ablated surface, a combination method was applied. Firstly, the crystals were treated with high laser power to ablate deep grooves, followed by a series of low-power laser pulses to melt and evaporate the fragments [Fig. 4(a)]. Figure 4(b) shows the topography after ablation with $F = 0.14$ J/cm^2, $N = 50$; lots of fragments were produced and grating structure formed. Then, low-power laser pulses (0.1 J/cm^2, $N = 200$) were used to smooth the surface by controlling the laser intensity and exposure time. Laser shots can produce surface melting over the entire irradiated surface area, and resolidification of this surface melt results in a smooth surface [Fig. 4(c).]. Following an increase in the number of irradiation pulses ($N = 500$), an even smoother surface was seen, as shown in Fig. 4(d). A magnified image showing the nanoscale features of such smooth surfaces is provided in Fig. 4(e).

In conclusion, laser interference ablation has been demonstrated to fabricate nanostructures on organic crystals. The effects of the laser fluence and the number of applied pulses on the laser-induced surface topography have been studied. Clean and smooth grating structures based on organic crystals have been fabricated using the direct writing method. The findings indicate that fragments of crystals with different morphologies can be produced, and these fragments can be well controlled and eliminated. Thus, the results show significant potential for fabrication of crystal devices.

This work was supported by the National Natural Science Foundation of China (NSFC) under Grant No. 90923037, 973 Project (2011CB013005), and Graduate Interdisciplinary Fund of Jilin University (No. 2011J008)

References

1. D. Fichou, S. Delysse, and J. M. Nunzi, Adv. Mater. **9**, 1178 (1997).
2. H. H. Fang, Q. D. Chen, R. Ding, J. Yang, Y. G. Ma, H. Y. Wang, B. R. Gao, J. Feng, and H. B. Sun, Opt. Lett. **35**, 2561 (2010).
3. H. H. Fang, Q. D. Chen, J. Yang, H. Xia, Y. G. Ma, H. Y. Wang, and H. B. Sun, Opt. Lett. **35**, 441 (2010).
4. C. Reese, M. E. Roberts, S. R. Parkin, and Z. A. Bao, Appl. Phys. Lett. **94**, 202101 (2009).
5. H. H. Fang, J. Yang, R. Ding, Q. D. Chen, L. Wang, H. Xia, J. Feng, Y. G. Ma, and H. B. Sun, Appl. Phys. Lett. **97**, 101101 (2010).
6. C. Reese and Z. N. Bao, J. Mater. Chem. **16**, 329 (2006).
7. R. J. Tseng, R. Chan, V. C. Tung, and Y. Yang, Adv. Mater. **20**, 435 (2008).
8. A. Ancona, S. Döring, C. Jauregui, F. Röser, J. Limpert, S. Nolte, and A. Tünnermann, Opt. Lett. **34**, 3304 (2009).
9. M. Huang, F. L. Zhao, Y. Cheng, N. S. Xu, and Z. Z. Xu, Acs Nano **3**, 4062 (2009).
10. X. P. Zhang, T. R. Zhai, Z. G. Pang, and F. Dou, Adv. Mater. **23**, 1860 (2011).
11. M. Stroisch, T. Woggon, U. Lemmer, G. Bastian, G. Violakis, and S. Pissadakis, Opt. Express **15**, 3968 (2007).
12. J. Ren, M. Kelly, and L. Hesselink, Opt. Lett. **30**, 1740 (2005).
13. B. Pivac, P. Dubcek, S. Milosevic, N. Krstulovic, Z. Kregar, and S. Bernstorff, Appl. Surf. Sci. **257**, 5358 (2011).
14. P. Dittrich, R. Bartlome, G. Montemezzani, and P. Gunter, Appl. Surf. Sci. **220**, 88 (2003).
15. R. Kabe, H. Nakanotani, T. Sakanoue, M. Yahiro, and C. Adachi, Adv. Mater. **21**, 4034 (2009).
16. J. Yang, H. H. Fang, R. Ding, S. Y. Lu, Y. L. Zhang, Q. D. Chen, and H. B. Sun, J. Phys. Chem. C **115**, 9171 (2011).
17. M. Huang, F. L. Zhao, Y. Cheng, N. S. Xu, and Z. Z. Xu, Phys. Rev. B **79**, 125436 (2009).